

Finite driving rates in interface models of Barkhausen noise

S. L. A. de Queiroz* and M. Bahiana†

*Instituto de Física, Universidade Federal do Rio de Janeiro,
Caixa Postal 68528, 21945-970 Rio de Janeiro RJ, Brazil*

(October 24, 2018)

We consider a single-interface model for the description of Barkhausen noise in soft ferromagnetic materials. Previously, the model had been used only in the adiabatic regime of infinitely slow field ramping. We introduce finite driving rates and analyze the scaling of event sizes and durations for different regimes of the driving rate. Coexistence of intermittency, with non-trivial scaling laws, and finite-velocity interface motion is observed for high enough driving rates. Power spectra show a decay $\sim \omega^{-t}$, with $t < 2$ for finite driving rates, revealing the influence of the internal structure of avalanches.

I. INTRODUCTION

The Barkhausen effect [1] constitutes a useful, non-destructive probe into the domain structure of soft ferromagnetic materials. By ramping an externally applied magnetic field within appropriately chosen ranges of intensity and driving rate, one causes microscopic domain wall motions, i.e. magnetization jumps, within a sample. The consequent changes in magnetic flux, in turn, induce a time-dependent electromotive force $V(t)$ on a coil wrapped around the sample. Analysis of $V(t)$, assisted by suitable theoretical modeling, may provide insight both into the domain structure itself and its dynamical behavior.

Recent increased interest in the problem stems partly from the successful application of methods of non-equilibrium statistical mechanics, such as a Langevin description via Fokker-Planck equations [2] and avalanche models [3–14]. Though there is general agreement on the basic underlying mechanisms of Barkhausen noise, pinning down specific details to features of theoretical models has proved a complex task. For instance, while several formulations have focused on the motion of a single interface in a disordered medium [2,3,5,6], others have adopted a picture of nucleation of multiple domains in a random-field Ising system [4].

The rapid and discrete variation of the magnetization observed in experiments is a direct manifestation of the existence of different time scales. Often the magnetization jumps are regarded as instantaneous events, but this is a simplification that allows the description of a limited dynamical regime, as finite driving rates are known to affect several aspects of the hysteresis cycle.

Barkhausen noise is observed in the central part of the hysteresis cycle, near the coercive field where the magnetization process is mainly due to domain wall motion, so interface models are usually successful in describing the associated non-trivial scaling laws [3,5,6,12,14]. In this paper we study the evolution of a single two-dimensional interface as it advances driven at a finite rate. The scal-

ing of event sizes and durations is analyzed for different regimes of the driving rate.

II. MODEL; FINITE DRIVING RATES

Here we shall use the single-interface model introduced in Ref. [3] for the description of Barkhausen noise, with adaptations for a finite driving rate. The interface at time t is described, in space dimensionality d , by its height $h(\vec{\rho}_i, t)$, where $\vec{\rho}_i$ is the position-vector of site i in a $(d-1)$ -dimensional lattice. Here we consider only $d = 3$. At each t , the height function $h_i = h(\vec{\rho}_i, t)$ is assumed to be single-valued, thus the interface element corresponding to the d -dimensional position-vector $\vec{r}_i = (\vec{\rho}_i, h_i)$ may be unambiguously labeled by i . Simulations are performed on an $L^{d-1} \times \infty$ geometry, with the interface motion set along the infinite direction. Therefore finite-size effects are controlled by the length parameter L [6]. Each element i of the interface experiences a force of the form:

$$f_i = u(\vec{r}_i) + \frac{k}{\gamma} \left[\sum_{j=1}^{\gamma} h_{\ell_j(i)} - \gamma h_i \right] + H_e, \quad (1)$$

where

$$H_e = H - \eta M. \quad (2)$$

The first term on the RHS of (1) represents the pinning force, u , and brings quenched disorder into the model by being chosen randomly, for each lattice site \vec{r}_i , from a Gaussian distribution of zero mean and standard deviation R . Large negative values of u lead to local elements where the interface will tend to be pinned, as described in the simulation procedure below. The second term corresponds to a cooperative interaction among interface elements, assumed here to be of elastic (surface tension) type. In this term, $\ell_j(i)$ is the position of the j -th nearest neighbor of site i and γ is the coordination number of

the $(d - 1)$ -dimensional lattice over which the interface projects. The tendency of this term is to minimize height differences among interface sites: higher (lower) interface elements experience a negative (positive) force from their neighboring elements. The force constant k gives the intensity of the elastic coupling, and is taken here as the unit for f . The last term is the effective driving force, resulting from the applied uniform external field H and a demagnetizing field which is taken to be proportional to $M = (1/L^{d-1}) \sum_{i=1}^{L^{d-1}} h_i$, the magnetization (per site) of the previously flipped spins for a lattice of width L .

For actual magnetic samples, the demagnetizing field is not necessarily uniform along the sample, as implied in the above expression; even when it is (e.g. for a uniformly magnetized ellipsoid), η would depend on the system's aspect ratio. Therefore, our approach amounts to a simplification, which is nevertheless expected to capture the essential aspects of the problem. See Ref. [12] for a detailed discussion.

Here we use $R = 5.0$, $k = 1$, $\eta = 0.05$, the same values as in the $d = 3$ simulations of Ref. [6].

We start the simulation with a flat wall. All spins above it are unflipped. The applied field H is set to the saturation value of the effective field H_e , in order to minimize transient effects (see e.g. Figure 1 of Ref. [6]). The saturation H_e depends on R , k and η (not noticeably on L) [6], and can be found from small-lattice simulations. The force f_i is then calculated for each unflipped site along the interface, and each spin at a site with $f_i \geq 0$ flips, causing the interface to move up one step. The magnetization is updated, and this process continues, with as many sweeps of the whole lattice as necessary, until $f_i < 0$ for all sites, when the interface comes to a halt. The external field is then increased by the minimum amount needed to bring the most weakly pinned element to motion. The avalanche size corresponds to the number of spins flipped between two interface stops.

In line with standard practice [7–11] our basic time unit is one lattice sweep, during which the external field is kept constant, and all spins on the interface are probed sequentially as described above. In the adiabatic regime, the external field is kept constant for the whole duration of an avalanche, i.e. for as many sweeps as it takes until no unstable sites are found along the interface. It is then increased by the amount needed to flip the weakest one. At finite driving rates, the field is increased by a fixed amount, henceforth denoted Δ , at the start of each sweep while an avalanche is taking place. Eventually, no more unstable sites will be left, and then one proceeds as in the adiabatic regime, increasing the field as much as necessary to start a new avalanche. Calling δH this latter quantity, the time interval between the end of one event and the start of the next is then $\delta H/\Delta$.

In what follows, we usually collected samples of 10,000 avalanches for each simulation, and data analysis has always been performed with the whole sets of data; however, in figures such as scatter plots of duration versus

size we display only a representative subset, typically 500–1,000 events, in order to avoid unnecessary clutter.

III. SIZE AND DURATION DISTRIBUTIONS

We consider the single-interface model introduced in Ref. [3], initially in the adiabatic limit. In Ref. [6] we showed that, in the context of this model, the upper cutoff in the avalanche size distribution is simply a manifestation of finite-size effects, i.e. of the width L of the cross-section of our simulated systems perpendicular to the direction of interface advance. Fitting our data to the customary power-law form multiplied by an exponential decay, namely

$$P(s) \propto s^{-\tau} \exp(-s/s_0) \quad , \quad (3)$$

we had τ in the range 1.2–1.4 and $s_0 \propto L^u$, $u = 1.4 \pm 0.1$.

The above value for u is consistent with $1/\sigma_k \simeq 2/3$ [defined via $s_0 \sim k^{-1/\sigma_k}$, k being a generic demagnetization factor], found both from renormalization-group analysis and numerical simulations of the interface model of Refs. [5,12,14], provided one makes the identification $k \equiv 1/L^2$, as pointed out in Ref. [14].

We first investigate whether finite widths affect properties related to avalanche duration.

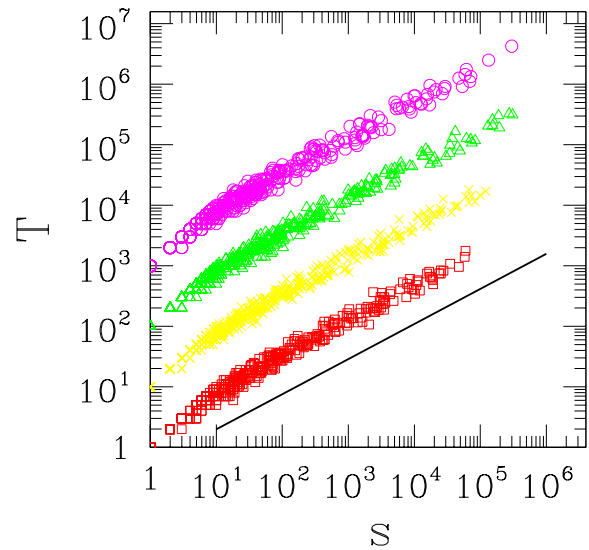


FIG. 1. Scatter plots of avalanche duration T (number of lattice sweeps) versus avalanche size (number of flipped sites), in the adiabatic regime. Bottom to top: $L = 40, 80, 160, 320, 500$ events displayed for each lattice L . Plots successively shifted upwards by a factor of 10 on vertical scale, to avoid superposition. Straight line has slope 0.58 (see text).

In Figure 1 one sees that in the adiabatic regime, apart from the L -dependent upper cutoff just mentioned, there is no distinguishable influence of finite lattice width on the distribution of avalanche durations T against size s .

For small events with $s \lesssim 10$ flipping sites, duration varies approximately linearly with size (collections of independent, localized flippings). For larger, collective events, non-trivial scaling takes hold; the relationship is described by the power law $T \sim s^{\sigma\nu z}$ (notation borrowed from Refs. [8,11]). Least-squares fits of data excluding small avalanches up to $s_{min} = 10 - 20$ give $\sigma\nu z = 0.58 \pm 0.01$, very similar to that previously obtained in simulations of the nucleation model, variously quoted as 0.57 ± 0.03 (Ref. [8]) or 0.58 (Ref. [11]). Thus, in this aspect at least, there is universality between single-interface and nucleation pictures.

Similar values of $\sigma\nu z$ are obtained also from slightly different variants of interface models [5,12–15]. In particular, simulations reported in Ref. [15] give $z = 1.56 \pm 0.06$ and the roughness exponent $\zeta = 0.75 \pm 0.02$, which, together with the scaling relation $\sigma^{-1} = \nu(2 + \zeta)$ (see Eqs. (34)–(37) of Ref. [12]), yields $\sigma\nu z = 0.57 \pm 0.02$.

Furthermore, the distribution of durations fits reasonably well to a power law with exponential tail, similarly to the size distribution Eq. (3):

$$P(T) \propto T^{-\alpha} \exp(-T/T_0) \quad , \quad (4)$$

where, from standard probability theory, $\alpha = 1 + (\tau - 1)/\sigma\nu z$ ($= 1.5 \pm 0.2$ from the values of τ and $\sigma\nu z$ quoted above). Indeed, analyzing the data shown in Fig. 1 one gets α in the range $1.3 - 1.5$. The cutoff T_0 is expected to scale with the size cutoff s_0 as $T_0 \sim s_0^{\sigma\nu z}$, therefore (with $s_0 \sim L^{1.4 \pm 0.1}$ [6]), one must have $T_0 \sim L^{0.81 \pm 0.06}$. Direct analysis of data gives the latter exponent varying in the range $0.65 - 0.9$, broadly compatible with this.

Next, we gauge the effects of varying driving rates on the size-duration relationship. For sufficiently fast driving rates, one expects coalescence of avalanches which would be separate events in the adiabatic regime.

We start by fixing $L = 80$. Δ , the external field increase at the start of each lattice sweep during an avalanche, is the driving rate. In Figure 2 one has $\Delta = 10^{-5}$, 5×10^{-5} , 7.5×10^{-5} , and 10^{-4} .

The plot for $\Delta = 10^{-5}$ is identical, apart from small fluctuations, to the corresponding one for $L = 80$ in the adiabatic regime, shown in Fig. 1. We have checked that the same happens for the in-between driving rates 10^{-m} , $m = 8, 7, 6$ (as expected). Again, least-squares fits give $\sigma\nu z = 0.58 \pm 0.01$ not only for the whole set of $\Delta = 10^{-5}$ data, but also for the initial parts (with $s \lesssim 10^5$) of those with faster driving rates. These latter plots will be discussed further ahead.

We conclude that, for $L = 80$ and within the range of $\Delta = 0 - 10^{-5}$, there is no influence of the driving rate on the $T - s$ relationship, including the maximum avalanche size, which remains at $s_{max} \simeq 10^5$. So far, the results: (i) $\tau = 1.3 \pm 0.1$; (ii) $\alpha = 1.5 \pm 0.2$ and (iii) independence

of behavior on driving rate (at least, within fairly well defined windows of Δ , for given L) show that the model under consideration shares the same universality class of the interface model discussed in Refs. [5,12–14], when dipolar interactions are neglected.

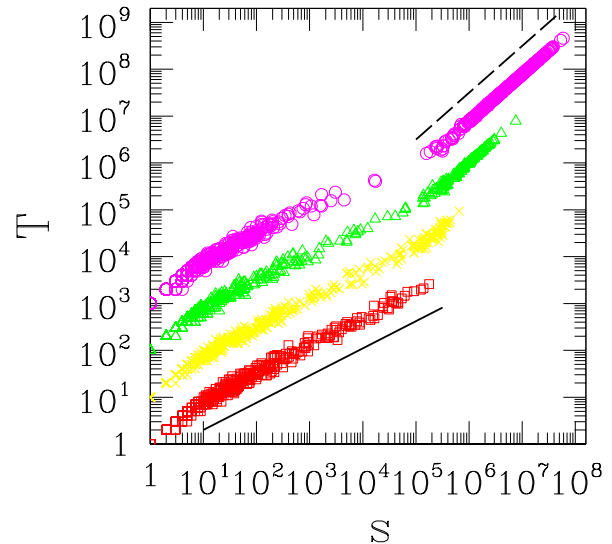


FIG. 2. Scatter plots of avalanche duration T versus avalanche size, for $L = 80$ and different driving rates Δ . Bottom to top: $\Delta = 10^{-5}$, 5×10^{-5} , 7.5×10^{-5} and 10^{-4} ; 500 events displayed for first three, 1,000 for $\Delta = 10^{-4}$. Plots successively shifted upwards by a factor of 10 on vertical scale, to avoid superposition. Full straight line has slope 0.58; dashed line has unitary slope (see text).

IV. RATE-DEPENDENT BEHAVIOR

We now investigate the different picture appearing for higher driving rates, already shown in Fig. 2. The scatter plot of duration against size for $\Delta = 5 \times 10^{-5}$ shows traces of a different behavior for $s > s_{max}$ as a higher slope develops at that point. As Δ is further increased, it can be seen that there is coexistence between non-trivial scaling for sizes \lesssim the adiabatic cutoff, and $T \sim s$ behavior (i.e. interface motion with a finite velocity) for larger avalanche sizes.

A qualitative explanation of the above results goes as follows. With $H_f(i)$ and $H_i(i + 1)$ being, respectively, external field at the end of the i -th avalanche and at the start of the $i + 1$ -th, typically the corresponding gaps $\delta H_i^{ad} \equiv H_i(i + 1) - H_f(i)$ in the adiabatic regime are larger than, say, several times Δ for $\Delta \leq 10^{-5}$; therefore few avalanches merge for such driving rates. For larger Δ more gaps are closed, and the distribution changes significantly.

In order to gain a quantitative understanding of this, at the same time checking for a possible L -dependence,

we study the probability distribution of δH^{ad} for different lattice widths.

In Fig. 3 we show the cumulative probability $P(\delta H^{ad} < \delta H_0)$ of δH^{ad} being smaller than δH_0 . Before analyzing the L -dependence of the curves, we focus on $L = 80$. One sees that $P(\delta H^{ad} < \delta H_0) \sim 3 \times 10^{-3}, 7 \times 10^{-2}$, respectively for $\delta H_0 = 10^{-5}, 10^{-4}$. From Fig. 2, the maximum avalanche duration is $T_{max} \sim 5 \times 10^3$, suggesting that the finite driving rate is irrelevant as long as the quantity $\mathcal{P} \equiv \mathcal{P}(L, \Delta) = T_{max} P(\delta H^{ad} < \Delta) \lesssim \mathcal{O}(10)$. On the contrary, for $\Delta = 10^{-4}$ Figs. 1 and 3 show that $\mathcal{P} \sim \mathcal{O}(100)$.

The inset of Fig. 3 shows that $P(\delta H^{ad} < \delta H_0)$ is, to a good approximation, a function of $L^x \delta H_0$, where the best collapse plots are obtained in the range $x = 1.9 \pm 0.1$. Though at this point we are not able to advance an argument, it may be that $x = 2$ exactly.

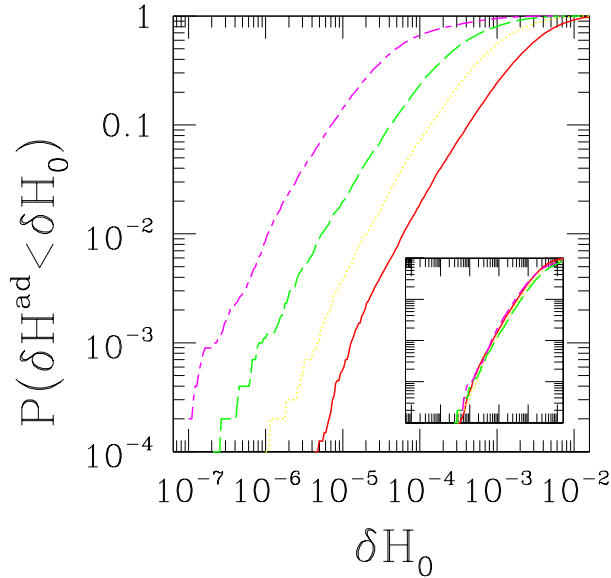


FIG. 3. Adiabatic regime: probability $P(\delta H^{ad} < \delta H_0)$ of the gap between consecutive avalanches being smaller than δH_0 , against δH_0 . Left to right: $L = 320, 160, 80$ and 40 , 40,000 events for $L = 40, 10,000$ for larger widths. Inset: $P(\delta H^{ad} < \delta H_0)$ against $(L/40)^x \delta H_0$, $x = 1.9$. Same ranges as main plot, on both horizontal and vertical axes (see text).

It is thus clear that as L increases the range of Δ for which adiabatic behavior dominates is shrunk. Recall that, on top of the scaling of probabilities with $L^x \delta H_0$, T_{max} (which scales with the cutoff T_0) also depends on L^v , $v \simeq 0.81$, see paragraph below Eq. (4). Thus, in the limit $L \rightarrow \infty$ one should have adiabatic-like properties only strictly at $\Delta = 0$. Before attaching much significance to this, one must bear in mind the main result of Ref. [6]: in the present model, L is closely correlated with the (average, or typical) domain size in experimental situations. Therefore, one does not have the usual

concern in the study of equilibrium second-order phase transitions, of trying to extract the thermodynamic limit from finite-size scaling: finite- L results must be analyzed in their own right. Nevertheless, it is crucial to investigate the size dependence of relevant quantities, as done here, in order to separate truly L -independent features from crossover behavior.

The departures from rate-independent behavior, as depicted in Fig. 2, require further analysis. A least-squares fit of data in that Figure for $\Delta = 10^{-4}$, $10 \leq s \leq 5 \times 10^4$ (the horizontal extent of the full line shown there) gives $\sigma \nu z = 0.58 \pm 0.01$. The events in this range of s are $\sim 20\%$ of the total number of avalanches; another 40% are small ones with $s < 10$, with the remaining 40% larger than 5×10^4 sites. The overall probability density $P(s)$ for $\Delta = 10^{-4}$, with the customary logarithmic binning, is displayed in Fig. 4, for the four driving rates of Fig. 2. The full straight line suggests that the $\Delta = 10^{-4}$ data with $1 \leq s \lesssim 5 \times 10^4$ can be fitted by a power law $P(s) \propto s^{-1.6}$. This larger effective value of τ can be understood by observing the depletion of events with sizes $10^4 - 10^5$ in the cross-over region of Fig. 2. Curves for $\Delta = 5 \times 10^{-5}$ and 7.5×10^{-5} display intermediate behavior, with only an incipient shoulder at $10^4 \lesssim s \lesssim 10^5$ for the former.

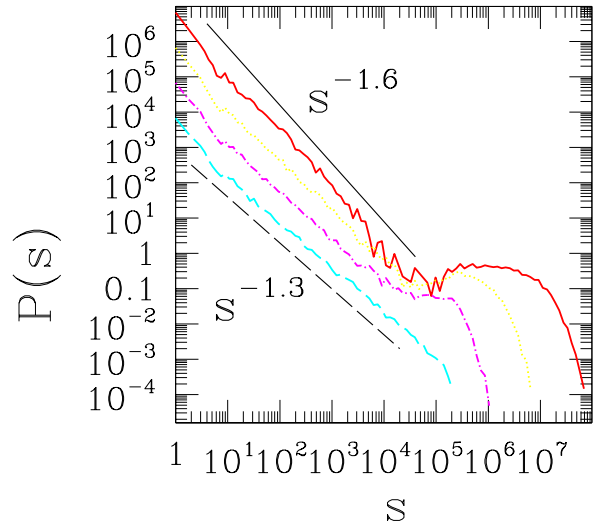


FIG. 4. Probability distributions of avalanche sizes for $L = 80$. Bottom to top: $\Delta = 10^{-5}, 5 \times 10^{-5}, 7.5 \times 10^{-5}$ and 10^{-4} . Curves successively shifted upwards by a factor of 10 on vertical scale, to avoid superposition (baseline is $\Delta = 10^{-5}$ plot). Straight lines have slopes as indicated, and are intended as guides to the eye.

We note that in earlier studies, both experimental [16] and numerical [17], it was found that the exponents τ of Eq. (3) and α of Eq. (4) decrease as driving rate increases, apparently in contradiction with the above. Also, a small

shoulder can be seen in the data for alloys under stress in Figure 1(a) of Ref. [14]. We comment on each of these in turn.

Firstly, recent work [14] shows that the FeSi alloys of Ref. [16] and, e.g., amorphous alloys under stress belong to different universality classes; while the former follow a mean-field description (giving rise to actual rate-dependent exponents), the latter display rate-independent exponents with values close to those found both for the present model, and for the model of Refs. [5,12–14] when dipolar interactions are neglected (see remarks at the end of Sec. III).

As regards the simulations of Ref. [17], it may be that the model used here does not belong to the same dynamical universality class as the (two-dimensional) random-field model with vacancies used there. However, examination of the data in Fig. 4 suggests an alternative explanation, as follows. Though fits of the straight-line parts of the distributions give τ increasing with Δ , fits of the whole sets of data to a form such as Eq. (3), with *two* free parameters (τ and s_0) in fact give *decreasing* values of τ for larger Δ , on account of the large- s shoulders. Of course, this happens at the expense of the quality of the fit; however, for less dramatic departures than those shown in the Figure, the loss of quality might not be obvious.

Finally, the incipient shoulders shown in Ref. [14] appear to be *bona fide* candidates for the above description, as they correspond to materials to which, so far, the present model seems to fit well. We believe that a re-examination of experimental and simulational raw data, in search of a coexistence of regimes, would be worthwhile. As pointed out in Ref. [17], “[a faster driving rate] overdrives weaker pinning centers thus rendering the occurrence of larger avalanches more probable”. For the present model this indeed happens, only it does so at the expense of depleting the histograms of occurrence of events \lesssim the respective maximum size for the adiabatic regime. We expect the present study to motivate further experimental and numerical investigation along these lines.

V. INTERMITTENCY

It is also important to analyze how the intermittency of events is gradually lost as more and more avalanches coalesce with increasing driving rate. This can be done by defining y as the fraction of time spent during avalanches. The duration of an avalanche being given by $T(i) = (H_f(i) - H_i(i))/\Delta$, the overall duration of a simulation with N events is $T_N = (H_f(N) - H_i(1))/\Delta$, therefore $y = (1/T_N) \sum_{i=1}^N T(i) = [\sum_{i=1}^N (H_f(i) - H_i(i))]/[H_f(N) - H_i(1)]$. In the adiabatic regime $\Delta = 0$, avalanches are instantaneous, and $y = 0$. As Δ is increased, avalanches will be observed part of the time, so $0 < y < 1$, and in the limit of large Δ , one expects that a depinning transi-

tion will lead to $y = 1$. Figure 5 shows the plot of $1 - y$ versus Δ for $L = 80$. The best non-linear fit of the whole set of points is given by $1 - y = \exp[-(\Delta/\Delta_0)^a]$ with the optimum values of the free parameters: $a = 1.2$ and $\Delta_0 = 1.57 \times 10^{-5}$. The inset shows the rate-independent regime corresponding to $y \ll 1$, where one clearly has $y \sim \Delta$. Such linearity is to be expected, as essentially the same events occur for any Δ in this interval: for a given avalanche, $H_f(i) - H_i(i)$ is proportional to Δ , while the denominator $H_f(N) - H_i(1)$ is unchanged. The fact that the best-fitting value of a is 1.2 indicates that the decay of $1 - y$ for large Δ is in fact faster than $\exp[-(\Delta/\Delta_0)^{1.2}]$, so one is having a compensation among the different regions of the plot, in order to minimize the overall deviation. A fit of the subset of data for $\Delta \geq 10^{-5}$ indeed gives $a \simeq 2$.

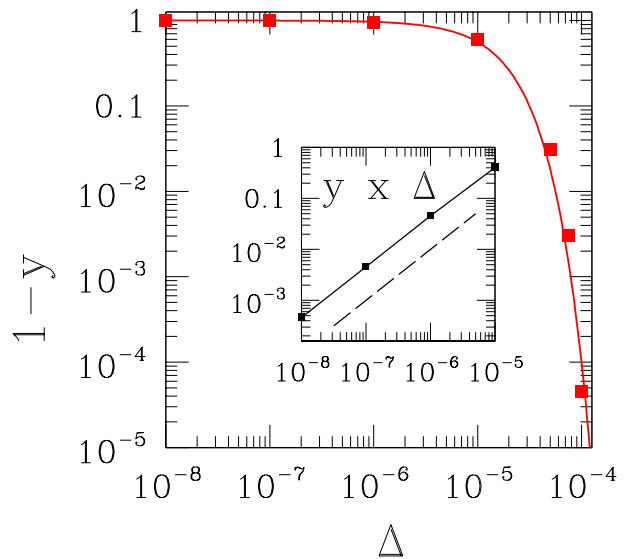


FIG. 5. Plot of $1 - y$ (y is the fraction of the total duration spent during avalanches) against driving rate Δ , for $L = 80$. Solid curve is fit to $1 - y = \exp[-(\Delta/\Delta_0)^a]$, $a = 1.2$, $\Delta_0 = 1.57 \times 10^{-5}$. Inset: y against Δ for slow driving; dashed line has unitary slope.

VI. POWER SPECTRA

Power spectra and their analysis are an important tool for the understanding of noise in disordered systems; specifically for the Barkhausen effect, see e.g. Ref. [11] for a recent survey of results and references; see also Ref. [18].

We shall always make $L = 80$ in this section. With the unit of time given by a lattice sweep, the maximum frequency to be analyzed is $\omega_M = 1/2$, as standard Fourier theory prescribes.

We attempt to concentrate on the non-trivial scaling regime. To this end, we recall from Fig. 2 that, whatever the driving rate, events of size $s \lesssim 10$ sites (of which there

is always a large fraction of the total) are collections of independent, localized flippings. Thus their duration is proportional to size. Therefore, when looking at power-spectrum data with frequencies $\omega \gtrsim 0.1$, one will have a strong input from such non-critical flippings. Though one might think of ways to expurgate the respective contributions, we shall simply restrict ourselves to the frequency region $\omega \leq 0.1$. As shown in the following, this still leaves a suitably wide window of observation, in what we call intermediate-frequency range (for $\omega \rightarrow 0$ the power spectrum goes flat, as details of the temporal series are washed out on long time scales).

The discussion of power spectra revolves mainly around the power t with which decay sets in, in the intermediate-frequency range: $P(\omega) \sim \omega^{-t}$. The following points were made in Ref. [11]: (1) While one has $t = 2$ for white noise and mean-field descriptions, and early studies of the Barkhausen effect predicted $t = (3-\tau)/\sigma\nu z$ ($= 2.9 \pm 0.2$ for the present model, with $\tau = 1.3 \pm 0.1$, $\sigma\nu z = 0.58 \pm 0.01$), it was found that for $\tau < 2$ one should have $t = 1/\sigma\nu z$ ($= 1.72 \pm 0.03$ here), instead of $(3-\tau)/\sigma\nu z$. Several experimental and simulational results were shown to be compatible with the latter finding. (2) It was remarked that the result of earlier calculations of the power spectrum [19] for sandpile models, which gave $P(\omega) \sim \omega^{-2}$ and were cited as an explanation for such behavior in (among other systems) Barkhausen noise, depends crucially on the assumption that the avalanche shape can be approximated by a box function: $V(t) = S/T$ ($0 < t < T$) for an avalanche of size S and duration T .

In the present model, one can tune the degree to which the internal structure of an avalanche is taken into account, by varying Δ . While for $\Delta = 0$ all events are seen as spikes of zero duration, the internal fluctuations within avalanches become much more noticeable as Δ increases, even still within the adiabatic regime. Recall that, for $\Delta = 10^{-5}$, $L = 80$, avalanches take up $\sim 40\%$ of the total duration of a simulation, see inset of Fig. 5.

Below, we set out to probe points (1) and (2). Accordingly, in Fig. 6 we plot the power spectra for $\Delta = 10^{-7}$ (deep within the adiabatic regime), 10^{-6} , 10^{-5} and 10^{-4} .

Starting from the slowest driving rate considered, one sees that disregarding the internal structure of avalanches indeed yields a dependence of the power spectrum on ω^{-2} . This is entirely consistent with point (2) above. The next graph, $\Delta = 10^{-6}$, is somewhat difficult to interpret on its own. However, the trend becomes clearer when the $\Delta = 10^{-5}$ data are taken into account: as more details of the intra-avalanche fluctuations enter into the spectrum, its decay becomes slower, $\sim \omega^{-1.5}$. Though the numerical values are somewhat off the mark, one definitely sees that the trend is towards $t = 1/\sigma\nu z$ when intra-avalanche correlations are considered, as opposed to the alternative $t = (3-\tau)/\sigma\nu z$. This is in support of point (1) above, showing that very likely the present model behaves similarly to the random-field one of Ref. [11], in this respect.

Finally, for $\Delta = 10^{-4}$ there is an apparent trend re-

versal; from a least-squares fit of data in the range of ω shown, one has the exponent 1.83 ± 0.01 . It must be recalled that one is then clearly in the coexistence regime explained above (that is, away from a purely intermittent, adiabatic framework); therefore there is strong influence of inter-avalanche correlations. It is then not surprising that the picture starts to differ e.g. from that of Ref. [11], where only inter-avalanche correlations were taken into account.

Clearly, more work is needed to sort out this latter point. As one goes deeper into the depinned regime, it may well be that the power spectrum decay returns to the ω^{-2} form characteristic of uncorrelated events. In such a scenario, the above value of $t = 1.83$ would in fact be an effective exponent, marking a crossover towards $t = 2$.

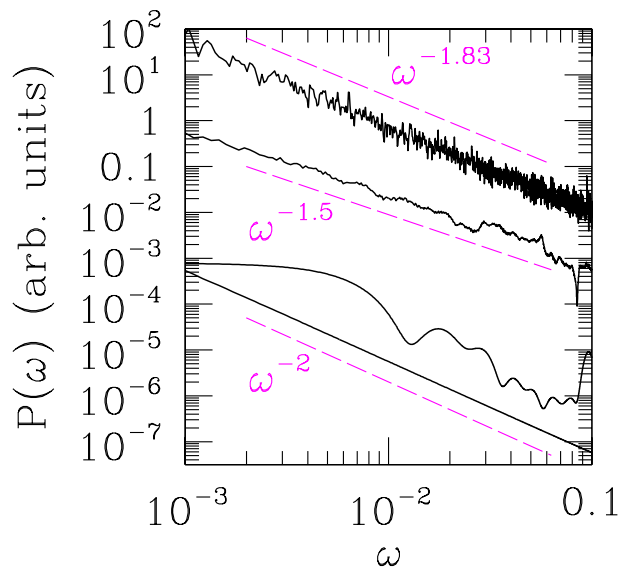


FIG. 6. Continuous lines: power spectra for $L = 80$ and various driving rates. Bottom to top, $\Delta = 10^{-7}$, 10^{-6} , 10^{-5} and 10^{-4} . The vertical coordinates have been shifted by differing amounts for each plot, so they could fit in a single graph. Dashed lines have slopes as indicated, and are intended as guides to the eye.

VII. CONCLUSIONS

We have used a single-interface model with an adjustable finite driving rate to simulate the time sequence of Barkhausen jumps of a three-dimensional system. Direct observation of duration as a function of size determines the existence of two dynamical regimes regarding the $\sigma\nu z$ exponent, that is, for low driving rates ($\Delta < \Delta_c(L)$), $\sigma\nu z = 0.58$ up to a limiting event size, and the avalanche dynamics is basically rate independent. For higher driving rates ($\Delta > \Delta_c(L)$) the previous regime coexists with one for which $\sigma\nu z = 1$. The rate

dependency of the second regime is evident as we analyze the probability distribution of avalanches sizes: for high driving rates it deviates considerably from the usual form, $P(s) \propto s^{-\tau} \exp(-s/s_0)$. The passage from one regime to the other is rather sharp, and the corresponding value of driving rate, Δ_c , depends on the system size: an infinite system will have a rate-independent dynamics for $\Delta = 0$ only, that is, $\Delta_c(\infty) = 0$.

Considering only the power-law portion of the $P(s)$ graphs for finite driving rate, we find exponents that increase with the driving rate, in apparent contradiction with previous theoretical and experimental results. On the other hand, when the fitting assumes a power law with an exponential cut-off, and the whole set of data is taken into account, the effective value of τ decreases as the driving rate is increased. It is clear though that this form does not provide an adequate description of the simulated data for $\Delta > \Delta_c$, so we believe that this may be at least part of the explanation for inconsistency in previously reported values of τ .

The power spectra for various driving rates clearly show that with increasing driving rates, intra-avalanche correlations become more relevant, as the time scale involved reveals details of events occurring with a finite duration. A direct consequence is the relation $P(\omega) \sim \omega^{-t}$ observed: as the internal structure of the avalanches is probed, t decreases from the value $t = 2$, characteristic of adiabatic time series.

In summary, we have studied the effect of a finite driving rate in the scaling properties of the Barkhausen noise. As our ultimate goal is the description of experimental results, it is important to understand the limitations involved in real experiments as compared to computational ones. In principle simulations may use any value for the driving rate, as well as any system size, or at least we may say that our choice of values is broad as compared to real experiments. A typical experiment usually has driving rates spanning only one order of magnitude, and values of domain sizes predetermined by the fabrication conditions of the sample and applied stress. So, as the experiment is designed with these parameters, the scaling regime is basically already chosen. Any further comparison with theoretical or simulation results must be careful in the sense that the same regime has to be studied.

ACKNOWLEDGMENTS

The authors thank Belita Koiller and Mark Robbins for interesting discussions, and Brazilian agencies CNPq (grants # 30.1692/81.5 and 30.1057/90.7), FAPERJ (grants # E26-171.447/97 and # E26-151.869/2000) and FUJB-UFRJ for financial support. We thank a referee for interesting comments, and for drawing our attention to relevant references.

- [1] H. Barkhausen, Phys. Z. **20**, 401 (1919).
- [2] B. Alessandro, C. Beatrice, G. Bertotti and A. Montorsi, J. Appl. Phys. **64**, 5355 (1988); *ibid.* **68**, 2901 (1990)
- [3] J.S. Urbach, R.C. Madison, and J.T. Markert, Phys. Rev. Lett. **75**, 276 (1995).
- [4] O. Perković, K. Dahmen, and J.P. Sethna, Phys. Rev. Lett. **75**, 4528 (1995).
- [5] P. Cizeau, S. Zapperi, G. Durin, and H.E. Stanley, Phys. Rev. Lett. **79**, 4669 (1997).
- [6] M. Bahiana, Belita Koiller, S.L.A. de Queiroz, J. C. Denardin and R. L. Sommer, Phys. Rev. E **59**, 3884 (1999).
- [7] B. Tadić, Physica A **270**, 125 (1999).
- [8] O. Perković, K. A. Dahmen, and J.P. Sethna, Phys. Rev. B **59**, 6106 (1999).
- [9] B. Tadić, Physica A **282**, 362 (2000).
- [10] B. Tadić and U. Nowak, Phys. Rev. E **61**, 4610 (2000).
- [11] M.C. Kuntz and J.P. Sethna, Phys. Rev. B **62**, 11 699 (2000).
- [12] S. Zapperi, P. Cizeau, G. Durin, and H. E. Stanley, Phys. Rev. B **58**, 6353 (1998).
- [13] G. Durin and S. Zapperi, J. Appl. Phys. **85**, 5196 (1999).
- [14] G. Durin and S. Zapperi, Phys. Rev. Lett. **84**, 4705 (2000).
- [15] H. Leschhorn, T. Nattermann, S. Stepanow, and L. H. Tang, Ann. Phys. (Leipzig) **6**, 1 (1997).
- [16] G. Bertotti, G. Durin and A. Magni, J. Appl. Phys. **75**, 5490 (1994).
- [17] B. Tadić, Phys. Rev. Lett. **77**, 3843 (1996).
- [18] G. Durin and S. Zapperi, e-print cond-mat/0106113 (2001).
- [19] H. J. Jensen, K. Christensen, and H. C. Fogedby, Phys. Rev. B **40**, 7425 (1989).